Scientific Research Publishing

Open Journal of Medicinal Chemistry, 2025, 15(1), 1-17
https://www.scirp.org/journal/ojmc
ISSN Online: 2164-313X
ISSN Print: 2164-3121

In Silico Exploration of New Inhibitors of Protein Kinases Containing an N-Phenylbenzamide Linker: A Combination of Docking and Molecular Dynamics Modeling, Pharmacophore Modeling and Virtual Screening

Aliaksandr Faryna*, Elena Kalinichenko

Institute of Bioorganic Chemistry, National Academy of Sciences of Belarus, Minsk, Belarus
Email: *farina@iboch.by

How to cite this paper: Faryna, A. and Kalinichenko, E. (2025) *In Silico* Exploration of New Inhibitors of Protein Kinases Containing an N-Phenylbenzamide Linker: A Combination of Docking and Molecular Dynamics Modeling, Pharmacophore Modeling and Virtual Screening. *Open Journal of Medicinal Chemistry*, **15**, 1-17.
https://doi.org/10.4236/ojmc.2025.151001

Received: November 22, 2024
Accepted: March 25, 2025
Published: March 28, 2025

Abstract

Protein kinase inhibitors (PKIs) are widely used in the treatment of various human cancers. Still, their applications are limited by drug resistance (both intrinsic and acquired) and adverse toxicity. Beyond traditional design approaches, computational methods like pharmacophoric analysis, docking, and molecular dynamics have proven effective in PKI development. In this study, novel N-phenylbenzamide derivatives were designed as potential protein kinase inhibitors using the virtual combinatorial chemistry method guided by the pharmacophoric properties of approved PKIs. The antikinase activity of 25 studied structures was evaluated *in silico* using molecular docking and molecular dynamics protocols. Docking scores against 102 kinase receptors were obtained and benchmarked against reference ligands. MMPBSA binding energies were evaluated for the 36 most promising complexes in a series of 2 ns and 20 ns simulations. The results show that the designed structures are promising scaffolds for the development of new effective anticancer drugs.

Keywords

Kinase Inhibitors, Rational Drug Design, Molecular Modeling, Pharmacophore

1. Introduction

Cancer remains one of the most formidable challenges to global health, accounting for millions of deaths worldwide each year. While the disease manifests in

various forms, the hallmark of cancer is uncontrolled cell growth and proliferation. Among the molecular players orchestrating these aberrant cellular behaviors, protein kinases emerge as key protagonists. These enzymes, which regulate critical signaling pathways, have become the focal point of modern cancer therapy due to their critical role in tumor initiation, progression, and metastasis [1]. In recent decades, the emergence of protein kinase inhibitors (PKIs) has revolutionized cancer treatment [2]-[4]. These targeted therapeutics act by inhibiting the activity of specific protein kinases, thus disrupting the signaling cascades that sustain malignant growth [5]. Imatinib, a breakthrough PKI developed to target the BCR-ABL fusion protein in chronic myeloid leukemia (CML), represents a paradigm-shifting success story in the field of oncology. Its introduction led to unprecedented responses in CML patients, effectively transforming a once-fatal disease into a manageable chronic condition [6]. The success of imatinib promoted intensive research into PKIs targeting various kinase-driven cancers as well as non-cancer conditions [7]. Constant identification of novel protein kinase targets and the revealing of target-related drug resistance mechanisms underscore the need for continuous innovation in PKI development. In recent decades, structure-based drug design (SBDD), accompanied by pharmacophore modeling and computation methods for binding affinity estimation, has emerged as an effective tool for the discovery and structure optimization of novel protein kinase inhibitors [8]. Crizotinib [9], Osimertinib [10], and Axitinib [11], as well as many other FDA-approved PKIs, are valuable examples of SBDD applications. On the other hand, *in silico* methods offer cost-effective means for rapid lead identification. Novel inhibitors of ZAP70 [12], CDK9 [13], and ABL-T315I [14] are recent examples of successful use of computational methods for the development of novel protein kinase inhibitors with *in vitro* validation.

In this study, 25 new N-phenylbenzamide derivatives were specifically designed and evaluated as potential protein kinase inhibitors against 102 protein kinases using molecular docking and molecular dynamics methods.

2. Materials and Methods

Study Design. Chemical compounds reflecting several chemical classes were specially designed to resemble the pharmacophore properties of type-2 protein kinase inhibitors [15]. Three-dimensional structures of these compounds were generated. In the first step, binding affinities of these structures to various protein kinase receptors were studied using molecular docking. The obtained binding affinities were compared to those of known inhibitors, and the best structures were taken to the next step, which was to estimate the binding energy of selected structures using molecular dynamics simulation followed by MM-GBSA workflow. For each structure, six experiments of binding energy estimation were conducted: five short-term 2 ns simulations and one 20 ns simulation. Given that a substantial proportion of approved kinase inhibitors are, in fact, type-1 inhibitors, which encompass a diverse array of chemical scaffolds, our receptor set was not exclusively

limited to type-2 receptors. Rather, it also included type-1 receptors to facilitate a more comprehensive investigation of the potential anti-kinase activity of the designed structures.

Docking. Structures of receptors were taken from the Protein Data Bank [16]. Three-dimensional structures of studied ligands were generated using the Cactus web server [17]. ADFR-suite was used for the preparation of the receptors and ligands for docking (prepare ligand, prepare receptor, and reduce programs) as well as for generating the coordinates and sizes of binding sites using coordinates of native ligands [18]. Qvina 2.1, with exhaustiveness set to 16, was used as docking software [19]. RMSDs for binding poses were calculated using RDKit (version 2020.09.1) Python package and custom scripting [20].

Molecular Dynamics. GROMACS (version 2022.4) was used as a molecular dynamics package [21]. Ligands were converted from Qvina's docking poses to sybyl mol2 format using OpenBabel [22] and protonated using Chimera [23]. Amber99sb-ildn force field was used for the simulations [24]. Ligands were parametrized to the Amber force field using the ACPYPE interface to Antechamber [25]. The protein-ligand system was prepared for the simulation using a dodecahedron box of 1 A, tip3p water model, and 0.15 mmol concentration of NaCl, followed by energy minimization and two equilibration steps (NPT and NVT) 200 ps each. The system state after the equilibration was used as a starting point for the separate production runs of different lengths. Parrinello-Rahman barostat and V-rescale thermostat were used for coupling. The Particle Mesh Ewald (PME) method was used for long-range electrostatic calculations. GMX-MMPBSA package was used to estimate binding energy [26]. The first 20 frames of the molecular dynamics trajectory of the protein-ligand complex were skipped. Interaction entropy was included in the binding energy calculations with the parameter "ie segment" being set to 25. The number of hydrogen bonds between receptor and ligand was estimated using the hbond module of the GROMACS package.

3. Results and Discussion

Design of Target Structures. Type-2 protein kinase inhibitors, such as imatinib, nilotinib, and sorafenib, bind to the inactive conformation of their target protein kinase. Such inactive conformations are characterized by the extension of the ATP-binding pocket from the active conformation to an adjacent, so-called 'allosteric' pocket. The examination of experimental structures of protein-ligand complexes reveals the most important pharmacophore properties of type-2 inhibitors. The structure of an inhibitor should contain a heterocyclic moiety that mimics the purine fragment, allowing it to bind in the ATP pocket of the inactive kinase. In the case of imatinib and nilotinib, 3-pyridyl-2-amino-pyrimidine is used to mimic the purine from the ATP molecule, while sorafenib uses pyridine and ponatinib uses imidazo-pyridazine. For the allosteric pocket, an amide group (in imatinib and nilotinib) or a carbamide group (in sorafenib) is necessary to form crucial hydrogen bonds, while a benzoic ring with different substituents provides van der

Waals interactions. The linker, which is typically a benzoic ring, provides the necessary orientation for the ATP and allosteric fragments of an inhibitor. In this study, based on the abovementioned considerations, we propose novel chemical structures specifically designed as type-2 protein kinase inhibitors. The key idea behind our design approach is to retain the N-phenylbenzamide linker-allosteric framework of imatinib while replacing the pyrimidine with a benzimidazole or purine fragment, followed by the introduction of some substituents, primarily in the allosteric benzene ring (Figure 1, Table 1), The strategy of utilizing the N-phenylbenzamide linker previously led us to the discovery of several chemical scaffolds able to suppress the growth of tumor cell lines [27] [28].

These structures were evaluated as protein kinase inhibitors using molecular docking and molecular dynamics.

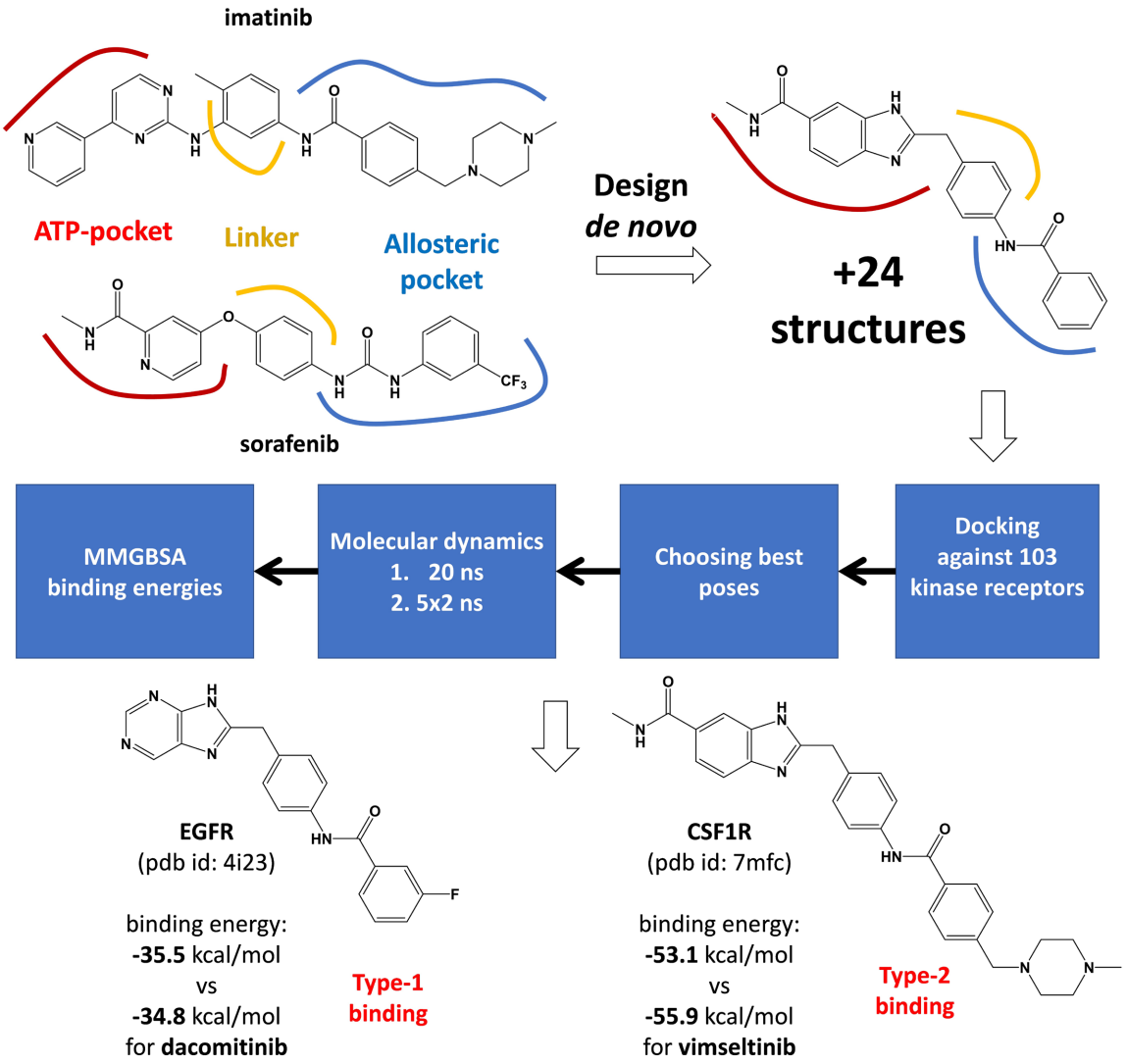

Figure 1. Summary of the design approach towards target benzimidazole and purine derivatives. The red line shows the ATP-pocket binding fragment of a molecule, the blue line shows the allosteric fragment and the orange line shows the linker.

Table 1. Structures of studied 4-methylbenzamide and benzimidazole or purine hybrids.

No.	Structure	No.	Structure
1a	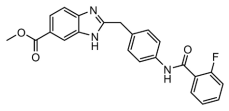	2a	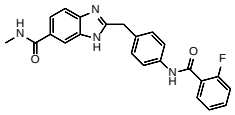
1b	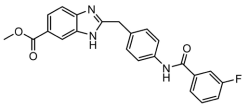	2b	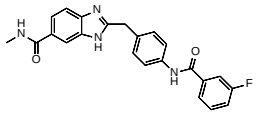
1c	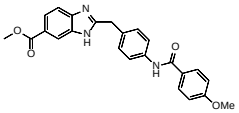	2c	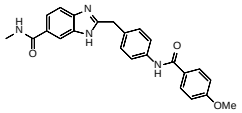
1d	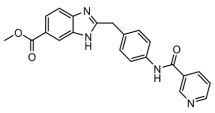	2d	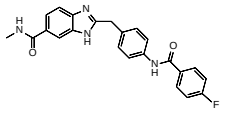
1e	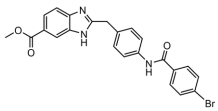	2e	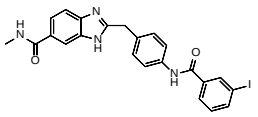
1f	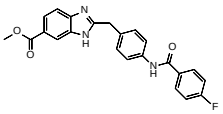	2f	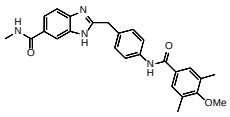
1g	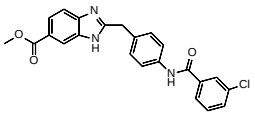	2g	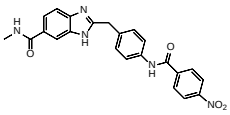
1h	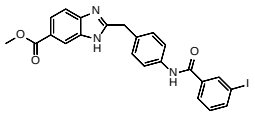	3a	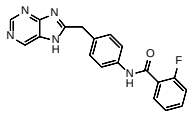
1i	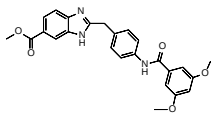	3b	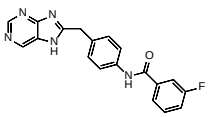
1j	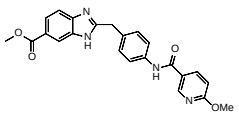	3c	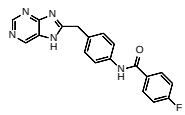
1k	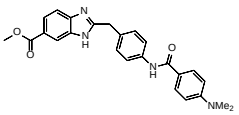	4a	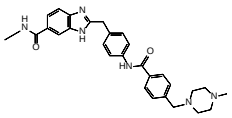
1l	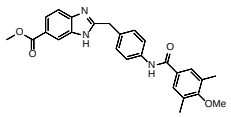	4b	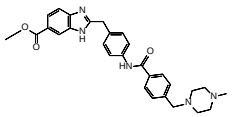
1m	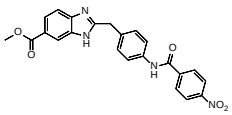		

Docking. The structures of 102 protein kinases from protein-ligand complexes of known inhibitors were used for docking. The structures were selected based on the approved protein kinase inhibitors list, followed by a manual examination of the PDB database. Selected complexes included both type-1 and type-2 inhibitors as native ligands.

First, docking of native ligands that were found in obtained PDB complexes was conducted to evaluate the performance of Qvina 2.1. The criteria for the docking pose of known ligands to be considered correct was the root mean squared deviation (RMSD) between atoms of the native ligand and the obtained docking pose. In our case, Qvina 2.1 was able to reproduce the binding pose of the original ligands according to the abovementioned criteria for 63 complexes out of 102 (62%, Figure 2).

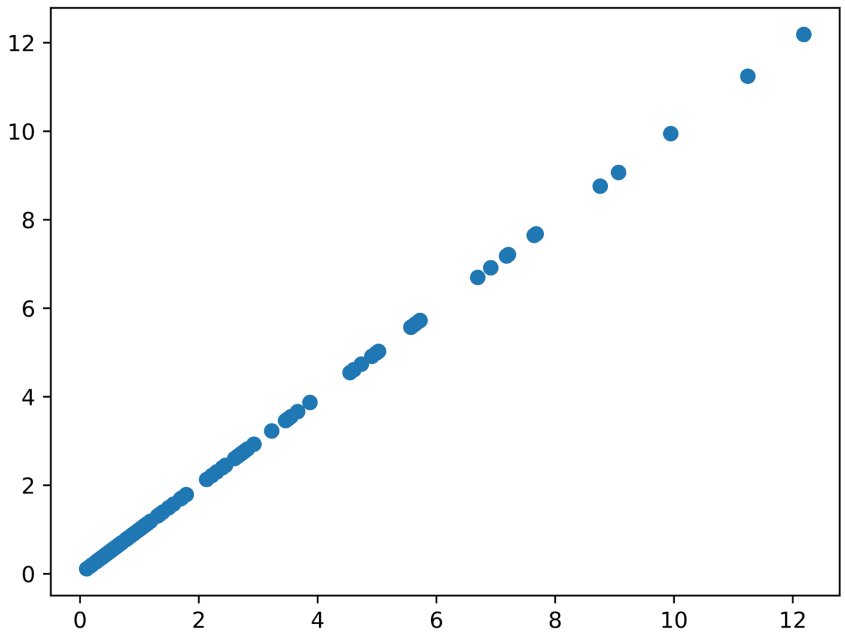

Figure 2. The distribution of root mean squared deviations (RMSD) of heavy atoms for the obtained docking poses of native ligands.

Studied structures were docked into kinase receptors. Obtained docking poses that showed binding affinity higher than those for native ligands having proper RMSD were of particular interest. These "high-affinity" poses were found for 19 receptors, most of which are of type-1 or type-1/2 (Figure 3).

Analysis of the structural features of the obtained compounds revealed that derivatives of N-methyl-1H-benzo[d]imidazole-6-carboxamide, series 2 (2a, 2b, 2d) showed the largest number of docking positions with high affinity in comparison with methyl esters (1a, 1b, 1f) or analogs containing purine bases 3a, 3b, 3c (Figure 4). It is also interesting to note that the presence of the fluorine atom in the meta position of the benzene ring has increased the affinity with the active center of the protein. However, replacing the fluorine atom in the para position with a methoxy group led to a sharp drop in activity.

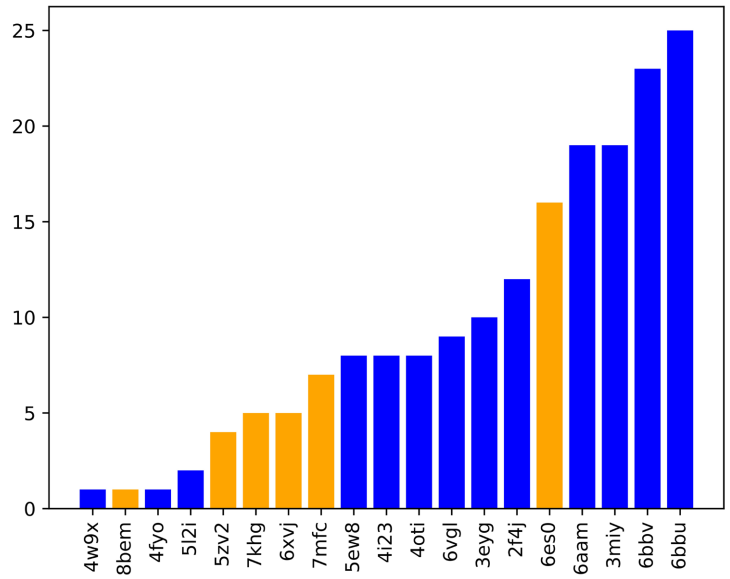

Figure 3. A number of docking poses of studied structures with binding energy equal to or greater than native ligands by PDB IDs of corresponding receptors. Blue bars are type-1 or type-1/2 receptors, and yellow bars are type-2 receptors.

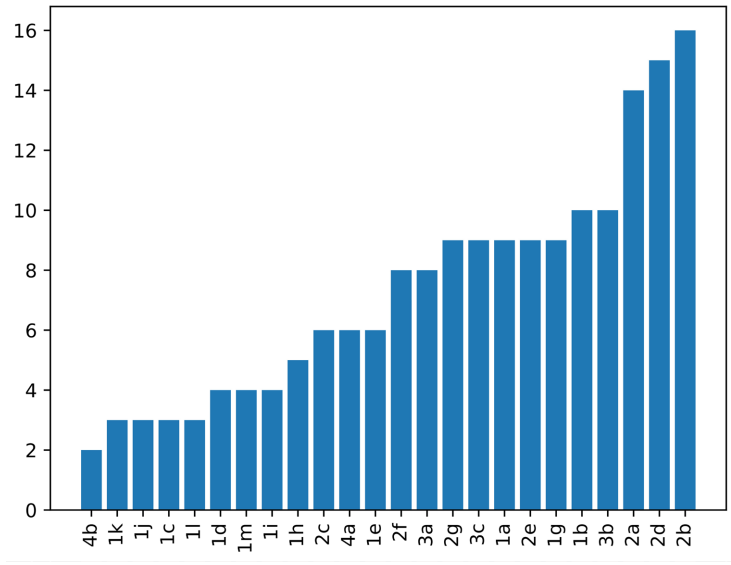

Figure 4. A number of docking poses of studied structures with binding energy equal to or greater than native ligands by structure ID.

Example visualization of docking poses of 2a for type-1 (6bbu, **Figure 5(A)**) and type-2 (6es0, **Figure 5(B)**) receptors suggests that for this structure, type-2 binding mode is more favorable as there is better alignment with native ligands [29] [30] (**Figure 5**). A notable difference exists in how the benzimidazole moiety of 2a is positioned relative to the adenine-binding region of ATP-pocket: it occupies this space only for type-2 receptor (6es0) while being pushed outside the location in the case of type-1 kinase conformation (6bbu). Also, a hydrogen bond was found for type 2 binding.

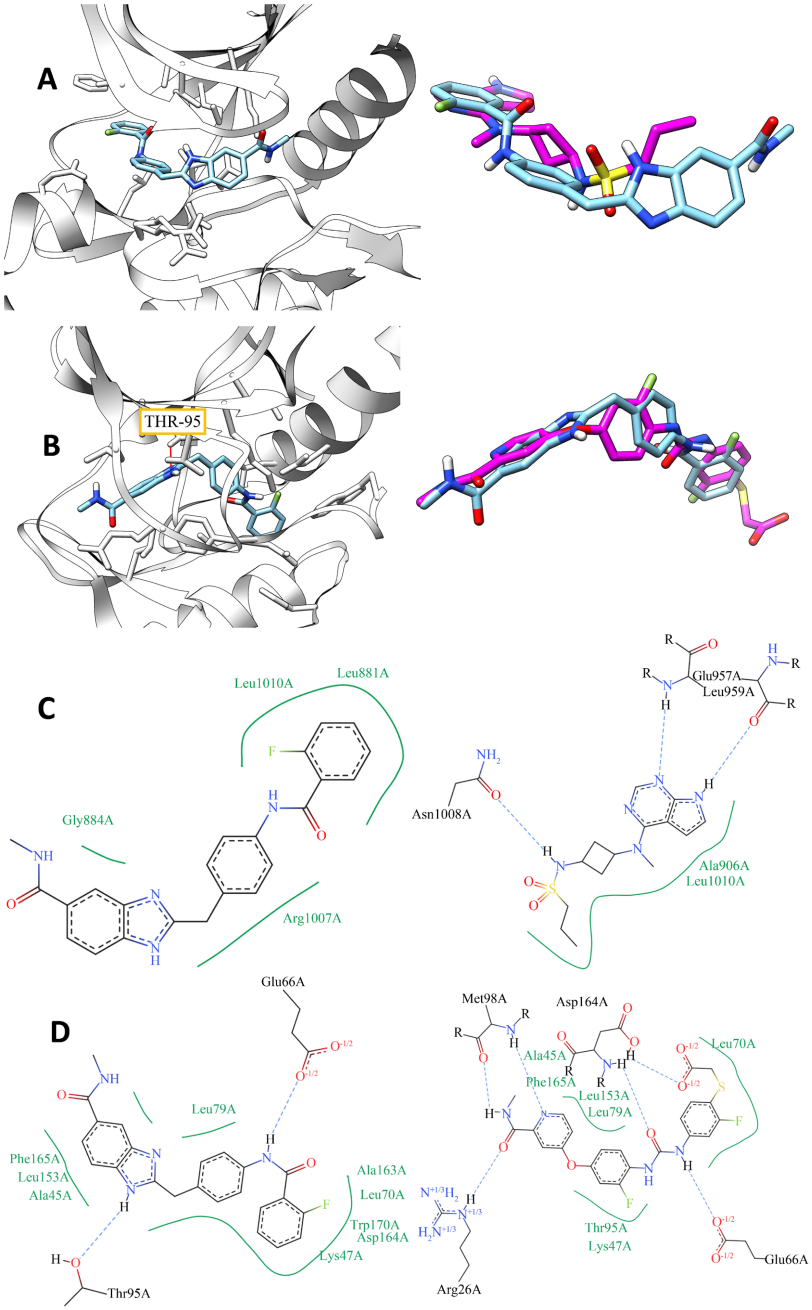

Figure 5. Visualization of highest ranked docking poses of 2a for type-1 (6bbu, A) and type-2 (6es0, B) receptors and their alignment with native ligands (pink). H-bonds found: THR-95 (6es0). Two-dimensional interaction diagram of 2a (left) and native ligand (right) for 6bbu receptor (C). Two-dimensional interaction diagram of 2a (left) and native ligand (right) for 6es0 receptor (D).

Studied structures from high-affinity docking poses and proceeded to the next step for the evaluation of binding energy using molecular dynamics workflow.

Molecular Dynamics. MM-PBSA binding energies against 12 kinase receptors were estimated for 71 studied structures and corresponding native ligands as a reference (a total of 83 protein-ligand complexes). The results are shown in **Table**

2 and visualized in Figure 6. In general, studied structures showed poorer binding energy if compared to known reference ligands. In most cases, binding energies for type-2 receptors for both reference ligands and studied structures were better than those for type-1 receptors. For two structures, 4a for the 2f4j receptor and 3b for the 4i23 receptor, binding energies that were estimated from the 20 ns simulation exceeded the values for the reference ligands. It should be noted that during the calculation, GMX-MMPBSA was not able to establish obtained entropy values as reliable, so entropy was not part of the final binding energy.

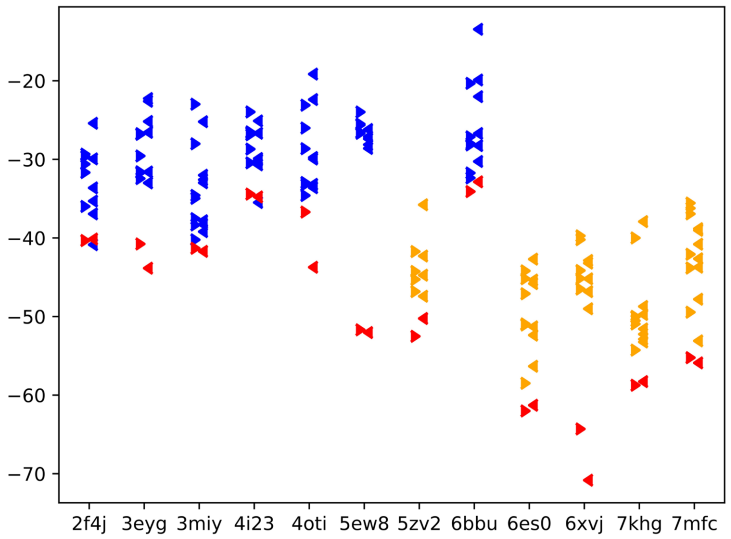

Figure 6. The estimated binding energy of studied structures and reference ligands by receptor. The binding energy obtained from the 20 ns is shown as "<" markers and the mean binding energy of five short 2 ns simulations is shown as ">" markers. Values for reference inhibitors are shown as red markers. Values for studied structures are shown as blue markers for type-1 kinase receptors and as orange markers for type-2 kinase receptors.

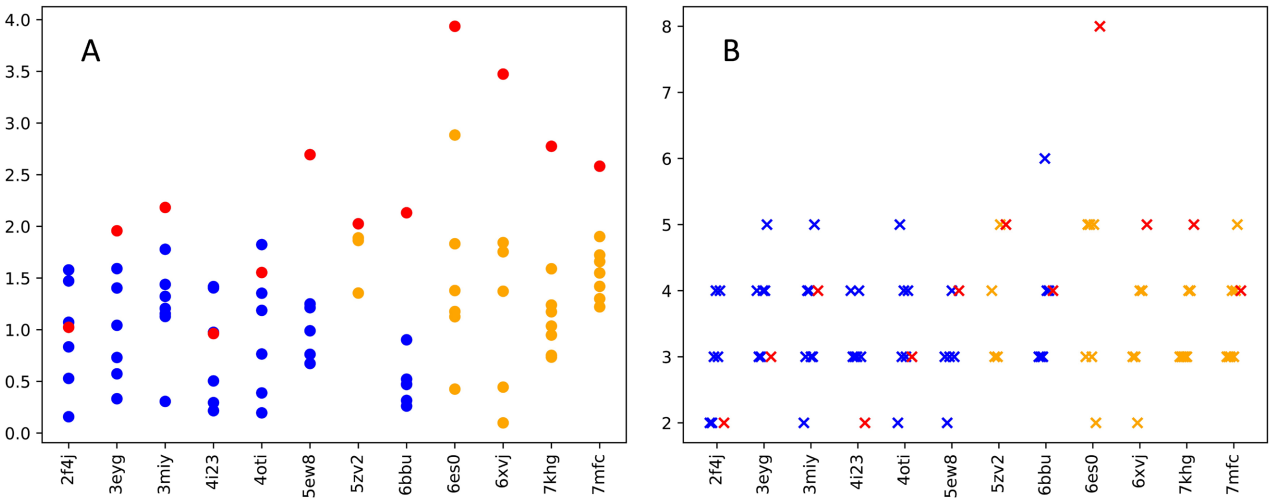

Figure 7. An average number of hydrogen bonds per frame (A) and a maximum number of hydrogen bonds (B) were estimated from 20 ns molecular dynamics trajectories of studied structures (blue markers for type-1 receptors, orange markers for type-2 receptors) and reference ligands (red markers).

Table 2. Obtained binding energies for studied structures and reference ligands, kcal/mol.

PDB	Lig.	Binding energy, 20 ns	Binding energy mean, 5 sim. x 2 ns	PDB	Ligand	Binding energy, 20 ns	Binding energy mean, 5 sim. x 2 ns
2f4j	3b	−33.63	−29.34	5zv2	1a	−47.42	−44.27
2f4j	1b	−25.41	−29.66	5zv2	2a	−44.74	−46.82
2f4j	2a	−36.94	−31.68	5zv2	2b	−42.3	−45.28
2f4j	2b	−29.94	−29.64	5zv2	2d	−35.78	−41.73
2f4j	2e	−35.31	−30.61	5zv2	native	−50.25	−52.52
2f4j	4a	−40.86	−35.99	6bbu	3a	−13.45	−20.33
2f4j	native	−40.14	−40.33	6bbu	1a	−19.9	−28.16
3eyg	3a	−22.61	−26.73	6bbu	1g	−22.02	−27.98
3eyg	1a	−31.61	−31.58	6bbu	2a	−26.71	−27.13
3eyg	1f	−22.26	−29.57	6bbu	2f	−30.27	−32.37
3eyg	2a	−33	−32.44	6bbu	4a	−28.25	−31.73
3eyg	2b	−25.18	−26.82	6bbu	native	−32.86	−34.1
3eyg	2d	−26.57	−31.71	6es0	1a	−45.81	−44.19
3eyg	native	−43.85	−40.76	6es0	2a	−45.36	−47.1
3miy	3b	−25.21	−22.98	6es0	2f	−51.31	−51.08
3miy	1b	−32.02	−28.02	6es0	2g	−52.37	−45.18
3miy	1g	−39.2	−37.54	6es0	4a	−56.33	−58.5
3miy	2b	−32.98	−34.96	6es0	4b	−42.7	−50.94
3miy	2e	−37.81	−38.35	6es0	native	−61.29	−62.01
3miy	2f	−32.59	−34.59	6xvj	2a	−46.83	−45.15
3miy	2g	−38.29	−40.24	6xvj	2b	−42.87	−39.73
3miy	native	−41.71	−41.32	6xvj	2d	−43.21	−40.22
4i23	3b	−35.49	−26.87	6xvj	2g	−45.2	−44.15
4i23	3c	−30.11	−23.97	6xvj	4a	−49.01	−46.5
4i23	1b	−25.11	−26.5	6xvj	native	−70.83	−64.31
4i23	1g	−29.89	−28.69	7khg	3a	−37.92	−40
4i23	2b	−30.7	−30.44	7khg	1a	−49.74	−50.06
4i23	2d	−26.68	−26.68	7khg	2b	−52.25	−50.53
4i23	native	−34.78	−34.42	7khg	2d	−48.72	−50.05
4oti	3a	−19.15	−23.11	7khg	2e	−51.58	−49.98
4oti	3c	−29.76	−26.01	7khg	2f	−53.24	−50.95
4oti	1a	−29.96	−34.6	7khg	2g	−52.88	−54.27
4oti	1b	−33.18	−33.23	7khg	native	−58.28	−58.75
4oti	1d	−22.39	−28.64	7mfc	1e	−43.72	−43.82
4oti	2b	−33.61	−32.95	7mfc	2a	−40.8	−35.56
4oti	native	−43.73	−36.7	7mfc	2b	−42.65	−36.22
5ew8	3a	−26.2	−23.98	7mfc	2d	−39.03	−36.94
5ew8	3c	−27.13	−25.63	7mfc	2e	−38.82	−42.08
5ew8	2a	−28.61	−26.54	7mfc	2g	−47.8	−43.83
5ew8	2b	−27.39	−25.51	7mfc	4a	−53.1	−49.45
5ew8	2d	−28.13	−26.69	7mfc	native	−55.9	−55.24
5ew8	native	−52.04	−51.69				

Table 3. The number of hydrogen bonds found between receptor and ligands during molecular dynamics simulation.

PDB	Ligand	Hydrogen bonds			PDB	Ligand	Hydrogen bonds		
		Avg	Min	Max			Avg	Min	Max
2f4j	3b	1.07	0	2	5zv2	1a	1.89	0	4
2f4j	1b	0.16	0	2	5zv2	2a	1.89	0	3
2f4j	2a	1.58	0	3	5zv2	2b	1.35	0	3
2f4j	2b	0.83	0	4	5zv2	2d	1.86	0	5
2f4j	2e	0.53	0	3	5zv2	native	2.03	0	5
2f4j	4a	1.47	0	4	6bbu	3a	0.32	0	3
2f4j	native	1.02	0	2	6bbu	1a	0.26	0	3
3eyg	3a	0.73	0	4	6bbu	1g	0.47	0	3
3eyg	1a	1.04	0	3	6bbu	2a	0.47	0	6
3eyg	1f	0.33	0	3	6bbu	2f	0.52	0	4
3eyg	2a	1.59	0	4	6bbu	4a	0.9	0	4
3eyg	2b	0.57	0	4	6bbu	native	2.13	1	4
3eyg	2d	1.4	0	5	6es0	1a	1.83	0	3
3eyg	native	1.96	0	3	6es0	2a	1.38	0	5
3miy	3b	0.31	0	2	6es0	2f	1.18	0	5
3miy	1b	1.13	0	3	6es0	2g	1.13	0	3
3miy	1g	1.44	0	4	6es0	4a	2.88	0	5
3miy	2b	1.32	0	4	6es0	4b	0.43	0	2
3miy	2e	1.15	0	3	6es0	native	3.94	1	8
3miy	2f	1.21	0	3	6xvj	2a	1.37	0	3
3miy	2g	1.78	0	5	6xvj	2b	0.44	0	3
3miy	native	2.18	1	4	6xvj	2d	0.1	0	2
4i23	3b	1.4	0	4	6xvj	2g	1.84	0	4
4i23	3c	0.22	0	3	6xvj	4a	1.75	0	4
4i23	1b	0.97	0	3	6xvj	native	3.47	1	5
4i23	1g	0.29	0	3	7khg	3a	1.17	0	3
4i23	2b	1.42	0	4	7khg	1a	0.73	0	3
4i23	2d	0.5	0	3	7khg	2b	1.59	0	3
4i23	native	0.96	0	2	7khg	2d	0.75	0	3
4oti	3a	0.2	0	2	7khg	2e	1.04	0	3
4oti	3c	1.82	0	5	7khg	2f	0.95	0	4
4oti	1a	1.19	0	3	7khg	2g	1.24	0	4
4oti	1b	0.77	0	4	7khg	native	2.77	1	5
4oti	1d	0.39	0	3	7mfc	1e	1.55	0	3
4oti	2b	1.35	0	4	7mfc	2a	1.3	0	3
4oti	native	1.55	0	3	7mfc	2b	1.66	0	3
5ew8	3a	0.76	0	3	7mfc	2d	1.42	0	4
5ew8	3c	0.67	0	2	7mfc	2e	1.22	0	3
5ew8	2a	1.25	0	3	7mfc	2g	1.9	0	4
5ew8	2b	1.21	0	4	7mfc	4a	1.72	0	5
5ew8	2d	0.99	0	3	7mfc	native	2.58	0	4
5ew8	native	2.69	0	4					

Analysis of molecular dynamics trajectory also showed that an average number of hydrogen bonds between receptor and ligand was, in most cases, greater for known inhibitors (Table 3, Figure 7(A)). Studied structures showed better average hydrogen bond numbers for receptors 2f4j (2a, 4a, 3b), 4i23 (1b, 2b, 3b) and 4oti (3c). All these receptors represent type-1 protein kinases. In terms of the maximum number of hydrogen bonds (Figure 7(B)), the results of studied structures and reference ligands could be, in general, considered as close. But in the case of type-2 receptors, known inhibitors showed a clear advantage, except for 7mfc, as structure 4a showed a maximum of 5 hydrogen bonds for this receptor, while native ligand vimseltinib showed 4 [31]. Nevertheless, vimseltinib maintained a higher average number of hydrogen bonds (2.58 versus 1.72 for compound 4a, Table 3).

Energy decomposition data is shown in Figure 8.

Comparing the energy decomposition data in relation to the energy of hydrogen bonds with amino acid residues in the active center of the 7mfc protein of the native ligand (Vimseltinib) and compound 4a showed a decrease in the binding energy with Tyr-99, Val-81, Met-71, Gly-183, and Cys-100. In the case of 4a, new interactions were found for Lei-22, Val-30, and Ile-70 residues, and there was a notable elevation in binding energy associated with Glu-67 (Figure 8). However, the appearance of new bonds apparently cannot compensate for the loss of binding with Leu-173, Ala-48, Lys-50, and Glu-98. As noted above, the average number of hydrogen bonds for Vimseltinib was 35% greater than for 4a (Table 3).

For the 4i23 receptor, structures 2b and 3b, containing a fluorine atom in the meta position of the benzene ring, showed a maximum number of hydrogen bonds of four instead of two for the reference ligand dacomitinib [32]. Also, the average number of hydrogen bonds for structures 2b and 3b was 1.5 times higher compared to the native ligand (Table 3). In general, the energy decomposition profile was similar for dacomitinib and structures 2b and 3b (Figure 8).

Comparison of the energy decomposition of the binding energy by amino acid residues of oncoprotein 2f4j with structures 2a, 2b, 3b, and 4a (Figure 8) showed their general similarity. However, the formation of strong additional interactions with Asn-322 is observed in the case of compound 2a, which probably affects the higher average number of hydrogen bonds compared to the reference ligand (1.58 versus 1.02) [33].

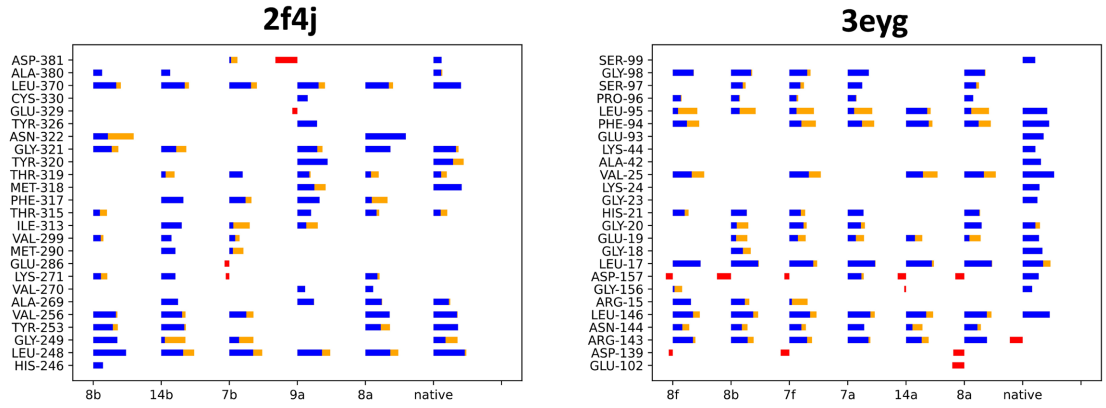

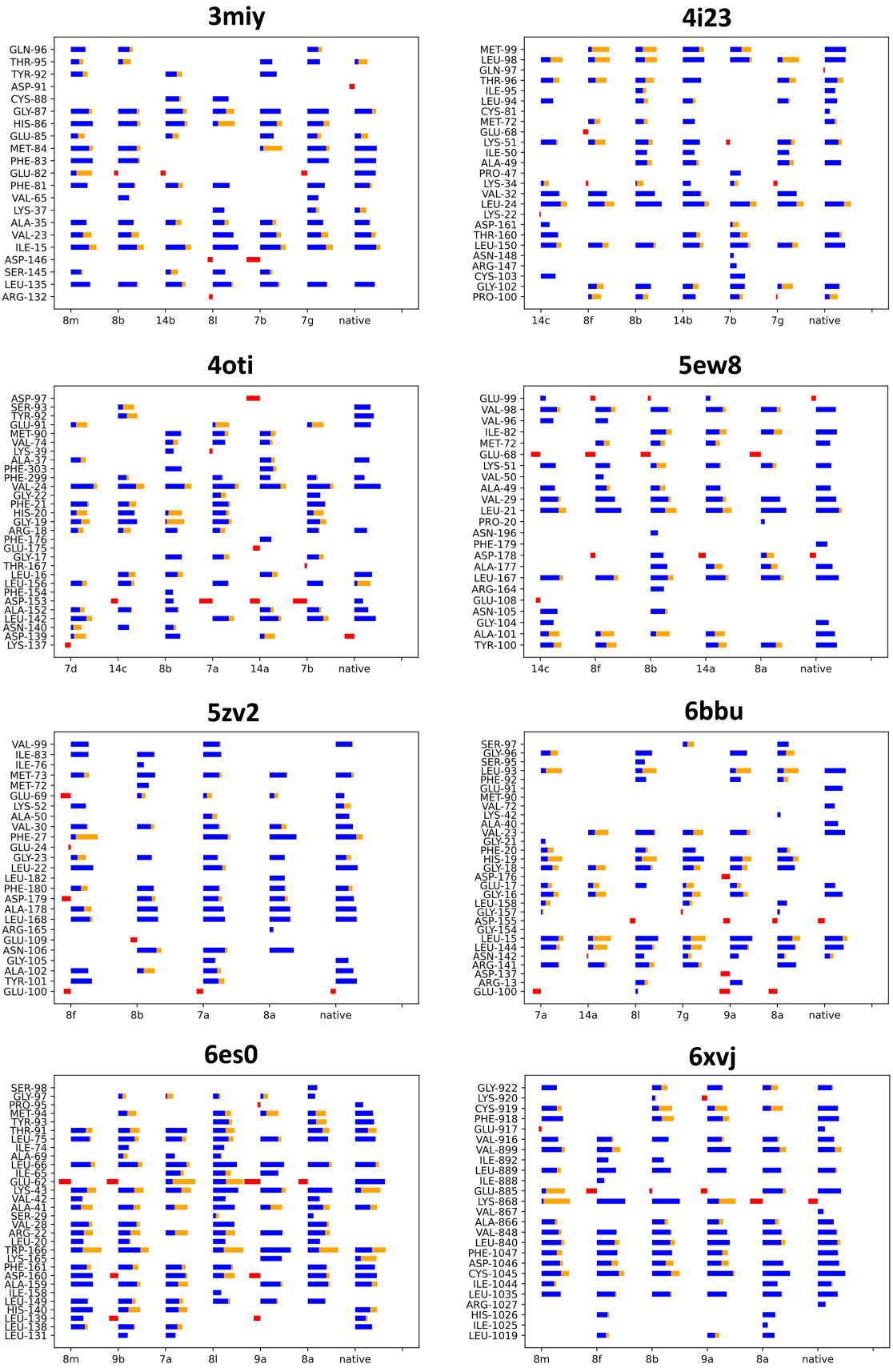
3miy
GLN-96
THR-95
TYR-92
ASP-91
CYS-88
GLY-87
HIS-86
GLU-85
MET-84
PHE-83
GLU-82
PHE-81
VAL-65
LYS-37
ALA-35
VAL-23
ILE-15
ASP-146
SER-145
LEU-135
ARG-132
8m 8b 14b 8l 7b 7g native
4i23
MET-99
LEU-98
GLN-97
THR-96
ILE-95
LEU-94
CYS-81
MET-72
GLU-68
LYS-51
ILE-50
ALA-49
PRO-47
LYS-34
VAL-32
LEU-24
LYS-22
ASP-161
THR-160
LEU-150
ASN-148
ARG-147
CYS-103
GLY-102
PRO-100
14c 8f 8b 14b 7b 7g native
4oti
ASP-97
SER-93
TYR-92
GLU-91
MET-90
VAL-74
LYS-39
ALA-37
PHE-303
PHE-299
VAL-24
GLY-22
PHE-21
HIS-20
GLY-19
ARG-18
PHE-176
GLU-175
GLY-17
THR-167
LEU-16
LEU-156
PHE-154
ASP-153
ALA-152
LEU-142
ASN-140
ASP-139
LYS-137
7d 14c 8b 7a 14a 7b native
5ew8
GLU-99
VAL-98
VAL-96
ILE-82
MET-72
GLU-68
LYS-51
VAL-50
ALA-49
VAL-29
LEU-21
PRO-20
ASN-196
PHE-179
ASP-178
ALA-177
LEU-167
ARG-164
GLU-108
ASN-105
GLY-104
ALA-101
TYR-100
14c 8f 8b 14a 8a native
5zv2
VAL-99
ILE-83
ILE-76
MET-73
MET-72
GLU-69
LYS-52
ALA-50
VAL-30
PHE-27
GLU-24
GLY-23
LEU-22
LEU-182
PHE-180
ASP-179
ALA-178
LEU-168
ARG-165
GLU-109
ASN-106
GLY-105
ALA-102
TYR-101
GLU-100
8f 8b 7a 8a native
6bbu
SER-97
GLY-96
SER-95
LEU-93
PHE-92
GLU-91
MET-90
VAL-72
LYS-42
ALA-40
VAL-23
GLY-21
PHE-20
HIS-19
GLY-18
ASP-176
GLU-17
GLY-16
LEU-158
GLY-157
ASP-155
GLY-154
LEU-15
LEU-144
ASN-142
ARG-141
ASP-137
ARG-13
GLU-100
7a 14a 8l 7g 9a 8a native
6es0
SER-98
GLY-97
PRO-95
MET-94
TYR-93
THR-91
LEU-75
ILE-74
ALA-69
LEU-66
ILE-65
GLU-62
LYS-43
VAL-42
ALA-41
SER-29
VAL-28
ARG-22
LEU-20
TRP-166
LYS-165
PHE-161
ASP-160
ALA-159
ILE-158
LEU-149
HIS-140
LEU-139
LEU-138
LEU-131
8m 9b 7a 8l 9a 8a native
6xvj
GLY-922
LYS-920
CYS-919
PHE-918
GLU-917
VAL-916
VAL-899
ILE-892
LEU-889
ILE-888
GLU-885
LYS-868
VAL-867
ALA-866
VAL-848
LEU-840
PHE-1047
ASP-1046
CYS-1045
ILE-1044
LEU-1035
ARG-1027
HIS-1026
ILE-1025
LEU-1019
8m 8f 8b 9a 8a native

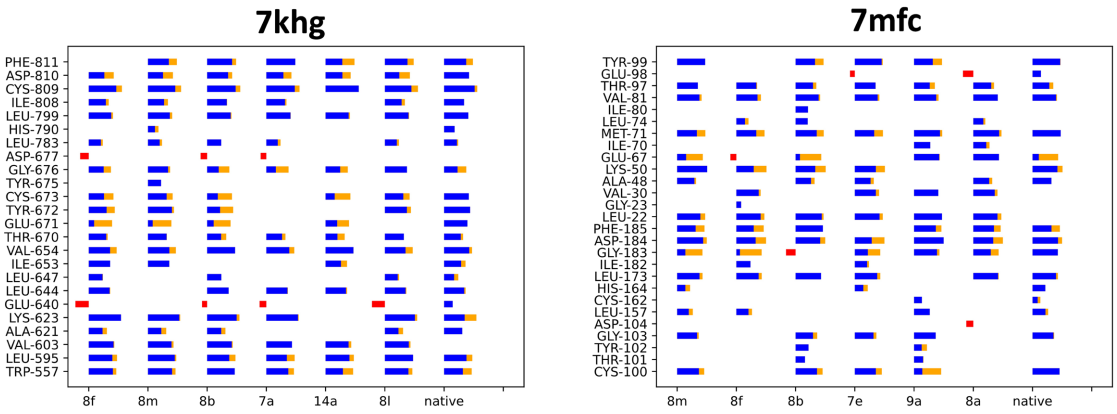

Figure 8. Energy decomposition of binding energy by residues. Negative values (favorable) are shown in blue, and positive (not favorable) are shown in red. Differences between the value obtained for a particular structure and the maximum value obtained found for all structures are shown in orange.

4. Conclusions

As a result of this study, 25 novel hybrids of 4-methylbenzamide and benzimidazole or purine were designed as protein kinase inhibitors and evaluated using molecular docking and molecular dynamics methods to estimate their binding affinity to 102 protein kinase receptors. It was shown that, in most cases, Qvina 2.1. is capable of accurately reproducing binding modes of known protein kinase inhibitors that were used as a reference.

For studied structures, docking poses with a score better than those of reference ligands were found for 19 receptors that mostly represent type-1 or type-1/2 kinase conformations. N-methyl-1H-benzo[d]imidazole-6-carboxamide (series 2) was the most common scaffold in docking poses with the highest binding affinity.

At the same time, MM-GBSA binding energies obtained from a series of molecular dynamics simulations were, in most cases, better for reference ligands.

Analysis of protein-ligand complexes of studied structures that were constructed by virtual combinatorial chemistry methods indicates the presence of effective intermolecular interactions leading to the blockade of the catalytic site of kinase enzymes. Comparison of the profiles of binding energy decomposition by amino acid residues of the active center of oncoproteins with pdb ids 2f4j, 4i23, 7mfc shows their general similarity between reference ligands and structures 2a, 2b, 3b, and 4a. In some cases, for studied structures, the formation of additional bonds was observed, which probably may improve binding energy.

The data obtained show that the use of the 4-methylbenzamide linker makes it possible to create promising lead structures for the development of effective multikinase drugs for antitumor therapy.

Funding

The research was funded by the National Academy of Sciences of Belarus within the State Scientific Investigation Program "Chemical processes, reagents and

technology, bioregulators and bioorganic chemistry, subprogram "Chemical basis of life processes", project No. 2.3.2.1.

Acknowledgements

Elena Kalinichenko coordinated the project and was responsible for general supervision and the review of the manuscript; Aliaksandr Faryna performed experimental work, including target structure design and molecular modeling studies, wrote and edited the manuscript. All authors have read and agreed to the published version of the manuscript.

Conflicts of Interest

The authors declare no conflicts of interest regarding the publication of this paper.

References

[1] Cicenas, J., Zalyte, E., Bairoch, A. and Gaudet, P. (2018) Kinases and Cancer. *Cancers*, **10**, Article 63. https://doi.org/10.3390/cancers10030063

[2] Liang, X., Wu, P., Yang, Q., Xie, Y., He, C., Yin, L., *et al.* (2021) An Update of New Small-Molecule Anticancer Drugs Approved from 2015 to 2020. *European Journal of Medicinal Chemistry*, **220**, Article 113473. https://doi.org/10.1016/j.ejmech.2021.113473

[3] Riegel, K., Vijayarangakannan, P., Kechagioglou, P., Bogucka, K. and Rajalingam, K. (2022) Recent Advances in Targeting Protein Kinases and Pseudokinases in Cancer Biology. *Frontiers in Cell and Developmental Biology*, **10**, Article 942500. https://doi.org/10.3389/fcell.2022.942500

[4] Zhang, Z., Liu, X., Zhao, L., Zhou, Y., Shi, J., Chen, W., *et al.* (2022) A Review on the Treatment of Multiple Myeloma with Small Molecular Agents in the Past Five Years. *European Journal of Medicinal Chemistry*, **229**, Article 114053. https://doi.org/10.1016/j.ejmech.2021.114053

[5] Pottier, C., Fresnais, M., Gilon, M., Jérusalem, G., Longuespée, R. and Sounni, N.E. (2020) Tyrosine Kinase Inhibitors in Cancer: Breakthrough and Challenges of Targeted Therapy. *Cancers*, **12**, Article 731. https://doi.org/10.3390/cancers12030731

[6] Lyseng-Williamson, K. and Jarvis, B. (2001) Imatinib. *Drugs*, **61**, 1765-1774. https://doi.org/10.2165/00003495-200161120-00007

[7] Roskoski, R. (2023) Properties of FDA-Approved Small Molecule Protein Kinase Inhibitors: A 2023 Update. *Pharmacological Research*, **187**, Article 106552. https://doi.org/10.1016/j.phrs.2022.106552

[8] Li, L., Liu, S., Wang, B., Liu, F., Xu, S., Li, P., *et al.* (2023) An Updated Review on Developing Small Molecule Kinase Inhibitors Using Computer-Aided Drug Design Approaches. *International Journal of Molecular Sciences*, **24**, Article 13953. https://doi.org/10.3390/ijms241813953

[9] Cui, J.J., Tran-Dubé, M., Shen, H., Nambu, M., Kung, P., Pairish, M., *et al.* (2011) Structure Based Drug Design of Crizotinib (PF-02341066), a Potent and Selective Dual Inhibitor of Mesenchymal-Epithelial Transition Factor (c-MET) Kinase and Anaplastic Lymphoma Kinase (ALK). *Journal of Medicinal Chemistry*, **54**, 6342-6363. https://doi.org/10.1021/jm2007613

[10] Yver, A. (2016) Osimertinib (AZD9291)—A Science-Driven, Collaborative Approach to Rapid Drug Design and Development. *Annals of Oncology*, **27**, 1165-1170. https://doi.org/10.1093/annonc/mdw129

[11] Kania, R.S. (2009) Structure-Based Design and Characterization of Axitinib. In: Li, R.S. and Stafford, J.A., Eds., *Kinase Inhibitor Drugs*, Wiley, 167-201.

[12] Zhao, H. and Caflisch, A. (2013) Discovery of ZAP70 Inhibitors by High-Throughput Docking into a Conformation of Its Kinase Domain Generated by Molecular Dynamics. *Bioorganic & Medicinal Chemistry Letters*, **23**, 5721-5726. https://doi.org/10.1016/j.bmcl.2013.08.009

[13] Wu, M., Han, J., Liu, Z., Zhang, Y., Huang, C., Li, J., *et al.* (2020) Identification of Novel CDK 9 Inhibitors Based on Virtual Screening, Molecular Dynamics Simulation, and Biological Evaluation. *Life Sciences*, **258**, Article 118228. https://doi.org/10.1016/j.lfs.2020.118228

[14] Al Shahrani, M., Gahtani, R.M., Abohassan, M., Alasmari, S. and Makkawi, M. (2023) Identification by Molecular Dynamic Simulation and *in Vitro* Validation of SISB-A1, N-[1-(4-Bromophenyl)-3-Methyl-1H-Pyrazol-5-Yl]-2-[(2-Oxo-4-Phenyl-2h-Chromen-7-Yl) Oxy], as an Inhibitor of the Abl^{T315I} Mutant Kinase to Combat Imatinib Resistance in Chronic Myeloid Leukemia. *Medical Oncology*, **40**, Article No. 316. https://doi.org/10.1007/s12032-023-02182-8

[15] Zhao, Z., Wu, H., Wang, L., Liu, Y., Knapp, S., Liu, Q., *et al.* (2014) Exploration of Type II Binding Mode: A Privileged Approach for Kinase Inhibitor Focused Drug Discovery? *ACS Chemical Biology*, **9**, 1230-1241. https://doi.org/10.1021/cb500129t

[16] Berman, H.M. (2000) The Protein Data Bank. *Nucleic Acids Research*, **28**, 235-242. https://doi.org/10.1093/nar/28.1.235

[17] NCI Chemical Identifier Resolver. http://cactus.nci.nih.gov/chemical/structure

[18] Ravindranath, P.A., Forli, S., Goodsell, D.S., Olson, A.J. and Sanner, M.F. (2015) Autodockfr: Advances in Protein-Ligand Docking with Explicitly Specified Binding Site Flexibility. *PLOS Computational Biology*, **11**, e1004586. https://doi.org/10.1371/journal.pcbi.1004586

[19] Alhossary, A., Handoko, S.D., Mu, Y. and Kwoh, C. (2015) Fast, Accurate, and Reliable Molecular Docking with Quickvina 2. *Bioinformatics*, **31**, 2214-2216. https://doi.org/10.1093/bioinformatics/btv082

[20] RDKit: Open-Source Cheminformatics. https://www.rdkit.org

[21] Abraham, M.J., Murtola, T., Schulz, R., Páll, S., Smith, J.C., Hess, B., *et al.* (2015) GROMACS: High Performance Molecular Simulations through Multi-Level Parallelism from Laptops to Supercomputers. *SoftwareX*, **1**, 19-25. https://doi.org/10.1016/j.softx.2015.06.001

[22] O'Boyle, N.M., Banck, M., James, C.A., Morley, C., Vandermeersch, T. and Hutchison, G.R. (2011) Open Babel: An Open Chemical Toolbox. *Journal of Cheminformatics*, **3**, Article No. 33. https://doi.org/10.1186/1758-2946-3-33

[23] Pettersen, E.F., Goddard, T.D., Huang, C.C., Couch, G.S., Greenblatt, D.M., Meng, E.C., *et al.* (2004) UCSF Chimera—A Visualization System for Exploratory Research and Analysis. *Journal of Computational Chemistry*, **25**, 1605-1612. https://doi.org/10.1002/jcc.20084

[24] Lindorff-Larsen, K., Piana, S., Palmo, K., Maragakis, P., Klepeis, J.L., Dror, R.O., *et al.* (2010) Improved Side-chain Torsion Potentials for the Amber Ff99SB Protein Force Field. *Proteins*: *Structure*, *Function*, *and Bioinformatics*, **78**, 1950-1958. https://doi.org/10.1002/prot.22711

[25] Sousa da Silva, A.W. and Vranken, W.F. (2012) ACPYPE—AnteChamber PYthon Parser InterfacE. *BMC Research Notes*, **5**, Article No. 367. https://doi.org/10.1186/1756-0500-5-367

[26] Valdés-Tresanco, M.S., Valdés-Tresanco, M.E., Valiente, P.A. and Moreno, E. (2021) Gmx_MMPBSA: A New Tool to Perform End-State Free Energy Calculations with Gromacs. *Journal of Chemical Theory and Computation*, **17**, 6281-6291. https://doi.org/10.1021/acs.jctc.1c00645

[27] Kalinichenko, E., Faryna, A., Kondrateva, V., Vlasova, A., Shevchenko, V., Melnik, A., *et al.* (2019) Synthesis, Biological Activities and Docking Studies of Novel 4-(arylaminomethyl)benzamide Derivatives as Potential Tyrosine Kinase Inhibitors. *Molecules*, **24**, 3543. https://doi.org/10.3390/molecules24193543

[28] Kalinichenko, E., Faryna, A., Bozhok, T. and Panibrat, A. (2021) Synthesis, *in Vitro* and *in Silico* Anticancer Activity of New 4-Methylbenzamide Derivatives Containing 2,6-Substituted Purines as Potential Protein Kinases Inhibitors. *International Journal of Molecular Sciences*, **22**, 12738. https://doi.org/10.3390/ijms222312738

[29] Vazquez, M.L., Kaila, N., Strohbach, J.W., *et al.* (2018) Identification of N-{cis-3-[Methyl(7H-pyrrolo[2,3-d]pyrimidin-4-yl)amino]cyclobutyl}propane-1-sulfonamide (PF-04965842): A Selective JAK1 Clinical Candidate for the Treatment of Autoimmune Diseases. *Journal of Medicinal Chemistry*, **61**, 1130-1152.

[30] Suebsuwong, C., Pinkas, D.M., Ray, S.S., Bufton, J.C., Dai, B., Bullock, A.N., *et al.* (2018) Activation Loop Targeting Strategy for Design of Receptor-Interacting Protein Kinase 2 (RIPK2) Inhibitors. *Bioorganic & Medicinal Chemistry Letters*, **28**, 577-583. https://doi.org/10.1016/j.bmcl.2018.01.044

[31] Smith, B.D., Kaufman, M.D., Wise, S.C., Ahn, Y.M., Caldwell, T.M., Leary, C.B., *et al.* (2021) Vimseltinib: A Precision CSF1R Therapy for Tenosynovial Giant Cell Tumors and Diseases Promoted by Macrophages. *Molecular Cancer Therapeutics*, **20**, 2098-2109. https://doi.org/10.1158/1535-7163.mct-21-0361

[32] Gajiwala, K.S., Feng, J., Ferre, R., Ryan, K., Brodsky, O., Weinrich, S., *et al.* (2013) Insights into the Aberrant Activity of Mutant EGFR Kinase Domain and Drug Recognition. *Structure*, **21**, 209-219. https://doi.org/10.1016/j.str.2012.11.014

[33] Young, M.A., Shah, N.P., Chao, L.H., Seeliger, M., Milanov, Z.V., Biggs, W.H., *et al.* (2006) Structure of the Kinase Domain of an Imatinib-Resistant Abl Mutant in Complex with the Aurora Kinase Inhibitor VX-680. *Cancer Research*, **66**, 1007-1014. https://doi.org/10.1158/0008-5472.can-05-2788